Feasibility study for large scale thermal convective flow measurements in building physics

Dirk Michaelis[1,*], Zhenming Peng[2], Peter Meyer[1], Thomas Brämer[1], Young Jin Jeon[1], Svenja Carrigan[2], Oliver Kornadt[2]

1: LaVision GmbH, Goettingen, Germany
2: Dept. of Building Physics / Energy-efficient Buildings, Rheinland-Pfälzische Technische Universität Kaiserslautern-Landau, Germany
* Correspondent author: dmichaelis@lavision.de

Keywords: thermal convective flow, building physics, large scale particle tracking velocimetry (PTV), Shake-the-Box, helium filled soap bubbles, data assimilation

ABSTRACT

The Department of Building Physics / Energy-efficient Buildings at the Rheinland-Pfälzische Technische Universität Kaiserslautern-Landau is about to put a novel research-building into commission, the "Small House III". Among other measurement equipment, a system for volumetric, large-scale, high-resolution flow velocity measurement should be utilized. In this paper, requirements for such a system are detailed, a suitable measurement system is proposed and a feasibility study for the verification of the system requirements is conducted. To this end, a tailored system for large-scale Lagrangian particle tracking ("Shake-the-Box") is applied to thermal convective flow measurements above an electric radiator close to a wall. As a result, it is found that the designed volumetric velocity measurement system is capable of successfully operating in the design environment without minimal disturbance of the low-speed convection flow. . After a relatively short setup time (about 5 hours, including camera setup, calibration and self-calibration) up to 10000 images at 50 Hz (200 seconds) have been recorded continuously. Shake-the-Box results show a decline of the number of tracked particles from initially 48000 to about 8000 (with a half-life span of about 100 seconds for the helium filled soap bubbles used for seeding). Applying fine scale reconstruction (data assimilation), a vector spacing of 4 mm could be achieved for instantaneous volumetric velocity snapshots. Averaging resulted in a 2 mm vector spacing with an average of 3300 particles per bin and 410 particles per bin for 1 mm vector spacing (with 75% bin overlap). Weaker particles could only be detected in front of a black background. Using a white background (default background for later applications), weak particles could not be detected as well, so the number of detected particles and the measurement volume decreased slightly compared to the black background. Overall, the feasibility study successfully confirmed the readiness of the measurement system for the intended use for "Small House III" measurements.

1. Introduction

The flow measurement system investigated in this study is intended for decentralized use in a research building at the Chair of Building Physics / Energy Building Optimization. This research building, called "Small House III" (Figure 1), houses a 2-zone climate chamber. In this chamber,

flow measurements will be conducted, covering three main fields of investigation: thermal comfort, moisture protection and natural ventilation.

Figure. 1 "Small House III", photo of the building (top) and CAD design for thermal comfort measurements (bottom)

Thermal comfort

Thermal comfort is influenced not only by building physics measurements, but also by physiological conditions and subjective perception. With the help of experimental studies in the climate chamber, the microclimate in the surroundings of people will be examined using different room air conditioning systems. In addition to the air and radiation temperature as well as the humidity, the flow speed in the people's immediate surroundings plays a central role. For this purpose, flow measurements are planned to be carried out in the immediate vicinity of a "Thermal

Manikin" with the help of the PTV system. The objective and reproducible results obtained in this way are then related to the subjective feelings of test subjects.

Moisture protection and energy-optimized construction

Moisture protection is essential to prevent structural damage and mould formation as well as to ensure comfort in the building. Investigations will cover the influences of convection and radiation as well as different uses, room geometries and boundary conditions with regard to temperature and humidity in order to gain essential knowledge about the room-side heat transfer to components of the building envelope.

Here, the PTV system is used to measure the air flow properties on the room-side surfaces. It is particularly important to examine air the flow conditions at a corner of the room. The results are primarily used to validate the Reynolds-averaged Navier–Stokes (RANS) simulations. An optimal measurement volume would span 0.5 m * 3 m * 0.3 m (length * height * width). To quantify the boundary layer at the wall, the optimal resolution is ~1 mm near the wall in natural convection, as this allows the viscous sublayer to be viewed in the averaged fields (Peng et al. 2023). For forced convection, e.g. with a ventilation system in the room, the optimal resolution at the wall would be < 1 mm (Peng et al. 2022). Far from the wall at a distance greater than 100 mm, a resolution of 2 mm is sufficient.

Air currents inside naturally ventilated rooms

In addition to mechanical ventilation in ventilation and air conditioning systems, air is always exchanged through leaky openings in the building envelope (e.g. through joints, windows or roller shutter boxes). Fresh outside air also flows into the building interior through classic window ventilation for the necessary air change.

This is called free or natural ventilation. For example, high air speeds sometimes occur during cross ventilation. The aim of the investigations is to analyse the flows in the room resulting from the overlapping of mechanical and free ventilation. Exact knowledge of the flow field allows, for example, the efficient use of component activation to support summer thermal protection. The results generated by the PTV system, therefore, serve as the basis for models for the dimensioning and development of new systems in which room air conditioning is supported by activated components.

Requirements for the flow measurement system

Up to now, velocity measurements in construction physics have been limited to planar measurements with small measurements areas or planar measurement with sub scale models

(Sattari 2015, Posner 2003). Just recently large-scale volumetric measurement has been applied with a breathing body model (Schröder 2022), however the applied measurement system had been installed behind transparent walls, which will not be possible for this application.

The intended use of the flow measurement system leads to the following system requirements:

1. Full-scale, large-scale, volumetric flow velocity measurement
2. Minimal safety requirements and low maintenance effort
3. No flow disturbance at inherent low convection velocities: no additional fans or heat-source can be positioned in the measurement chamber
4. Easy, quick and precise calibration
5. Quick, on-site data quality check
6. High spatial resolution for instantaneous and average velocity fields

The following system components have been selected to best meet these requirements:

1. Helium filled soap bubble seeding (Scarano 2015) with volumetric LED illumination, which allows safe, large scale volumetric measurements addressing requirements 1 and 2.
2. Liquid cooled LED's and cameras: the heat generated by cameras and LED-illumination is transported to chillers outside the measurement chamber using liquid cooling pipes, addressing requirement 3.
3. Bundle-adjustment pinhole calibration with a large calibration plate and volume self-calibration (Wieneke 2008) allows to meet requirement 4.
4. Shake-the-Box particle tracking allows quick data analysis (e.g. at least ten times faster than Tomographic PIV) (Schanz 2016), meeting requirement 5.
5. Averaging from particle tracking allows arbitrary high spatial resolution for average flow fields (limited by the available recording time in practise) (Schröder 2015). Also, data assimilation methods like VIC# (Jeon 2022) are used to gain an optimal spatial resolution for instantaneous velocity fields, targeting the final requirement number 6 from the above list.

In the following parts, the experimental setup and the measurement procedure are described briefly and results from data analysis are discussed shortly to evaluate the system performance regarding the stated requirements.

2. Experimental Setup
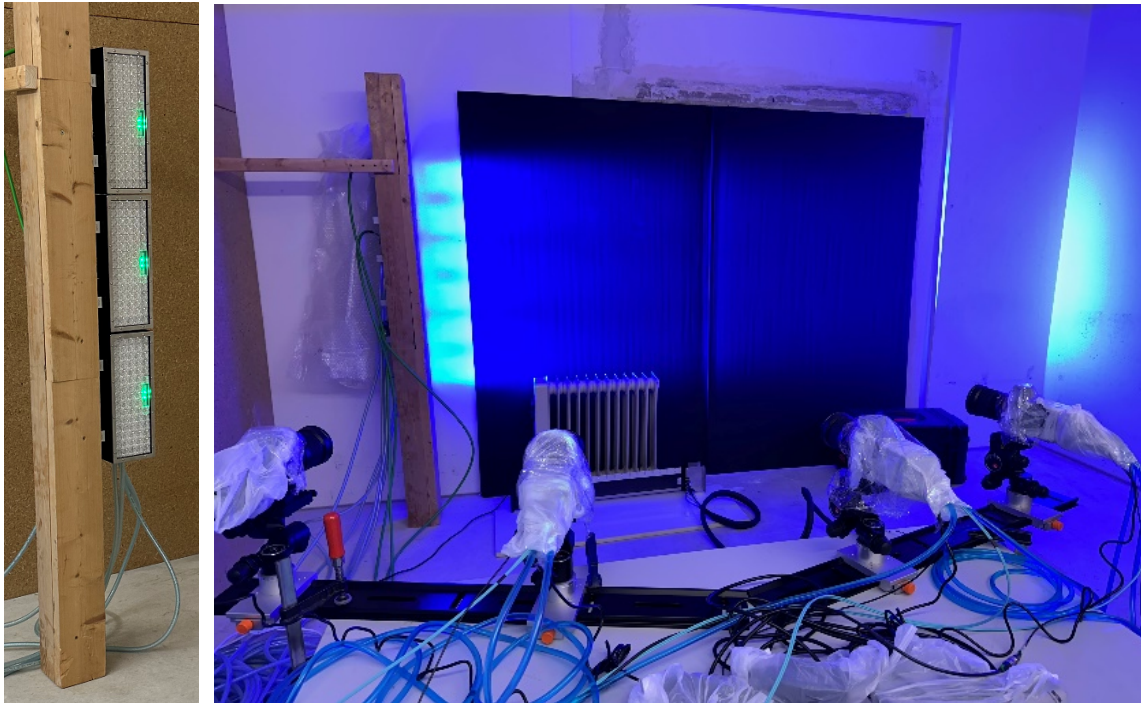
Figure. 2 Experimental setup: four water-cooled sCMOS cameras (right) are recording time resolved particle tracks from Helium filled soap bubbles which are illuminated by water-cooled LED's (left)

The measurement system from LaVision (Figure 2) included four water-cooled 5 Megapixel sCMOS cameras, three water-cooled LED-300 modules for pulsed volumetric illumination, 20 nozzles for Helium filled soap bubble generation (with about 300 μm diameter) at 30000 particles per second per nozzle and a system computer that allowed continuous time resolved recording at 50 Hz from all four cameras. The measurement volume was placed on top of an electrical radiator close to a black wall. In later measurements, the black wall was replaced by a white wall for half of the measurement area, to study the influence of the background on the quality of particle tracking.

3. Recordings and Analysis Procedures

Recordings were taken at 50 Hz with 1000 or 10000 images per recording. The given maximal convection velocity of about 0.5 m/s resulted in a maximum particle shift of about 45 voxels between successive images. This is on the higher side for optimal particle tracking. However, iterative forward-backwards tracking still allowed successful tracking of 50000 particles per time step. LED illumination was pulsed with 335 μs illumination time avoiding motion blur of the illuminated particles. The brightest bubbles were imaged with about 8000 to 10000 counts (on the 16-bit camera), yielding an excellent signal to noise ratio.

Figure. 3 2D-calibration plate for volumetric pinhole calibration. Five views at different locations and viewing angles have been recorded for bundle adjustment.

The initial perspective calibration was done using a large 1 m² 2D-calibration-plate (Figure 3), bundle adjustment of five different views of the calibration plate and a pinhole model. The calibration was refined using volume self-calibration [5] of a 1150 x 900 x 250 mm³ volume with three polynomial planes for each camera, reducing the initial calibration error of 0.14 pixel to an average remaining disparity of 0.04 voxel (max. 0.14 voxel).
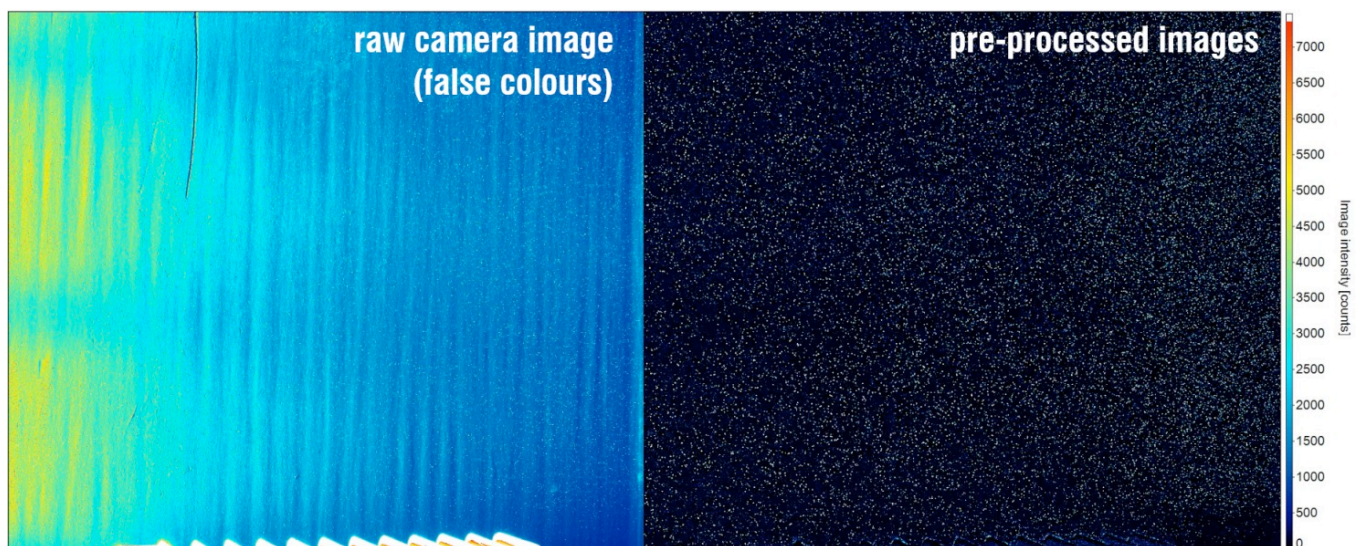
Figure. 4 recorded particle image: raw image (left), pre-processed image (right)

Image pre-processing was applied to the recorded particle images to remove the static background and increase the particle image quality. In the raw images, the background intensity from the black wall was up to 5000 counts where the LED light was touching the wall (Figure 4, left).

1. Subtract the sliding minimum over five time-steps for each pixel (before subtraction, the minimum is multiplied by a weighting factor: 1.02 for the black background and 1.04 for the white background. The idea behind this factor > 1.0 is, that the minimum contains (gaussian) noise, so that statistically the minimum is overestimated for 50% of the pixel. To avoid detecting noise as particles, at the potential cost of removing some true weak particles, the minimum is multiplied with a factor > 1.0. The resulting negative values are set to zero.

2. Subtract local sliding minimum over 4 pixels.

3. Normalize intensity over a sliding 300 pixel average and normalize all cameras to the average intensity of the first camera.

4. Slight Gaussian smoothing.

5. Subtract 30 counts.

6. Multiply result with 10 (increase dynamic range before back converting the float result to 16-Bit integer).

An exemplary result of the pre-processing chain, where the background has now been removed from the raw images, is shown in Figure 4, right.
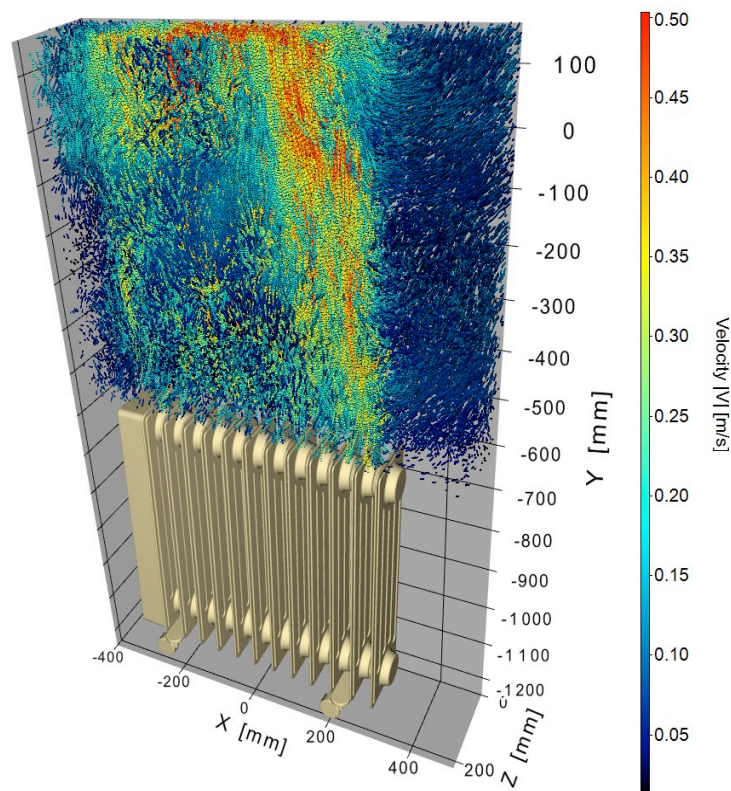
Figure. 5 Time-resolved Shake-the-Box particle tracking resulted in about 50000 tracked particles per time step.

Five passes of multi-pass Shake-the-Box [6] particle tracking have been applied to the pre-processed images to recover up to 47000 particle tracks per time step (Figure 5). In this experiment, the limiting factor for the seeding density was the seeding generation. Initial tests showed that even after 6 minutes of seeding generation the seeding density did not increase anymore.

4. Results

4.1. Particle tracking
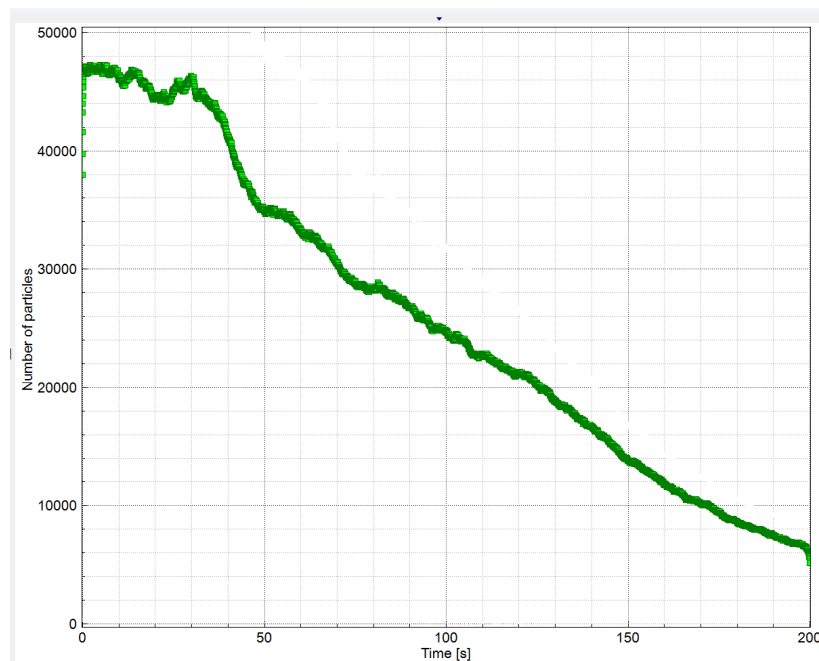
Figure. 6 Number of tracked particle over time using the recording with 10000 images. Collapsing bubbles reduce the number of tracked particles over time.

The seeding generator is switched off before particle image recording to avoid the influence of the fast bubble jets on the relatively slow convective flow from the radiator. For the recording with 10000 images at 50 Hz, the number of particles that can be tracked over time is shown in Figure 6. Initially, about 47000 particles have been tracked, decreasing to about 8000 particles at the end of the recording after 200 seconds. The half-life time of the particles is about 100 seconds, after which half of the particles have collapsed. It is important to note that for this initial test, the seeding particles have not been filled by helium but with air. The lifetime may be longer if helium is used so that the bubbles stay in the air for a longer time and do not collapse from touching the floor so easily. Also, increasing the air humidity could be used to improve the lifetime of the bubbles.

4.2. Conversion of particle tracks to a velocity vector grid
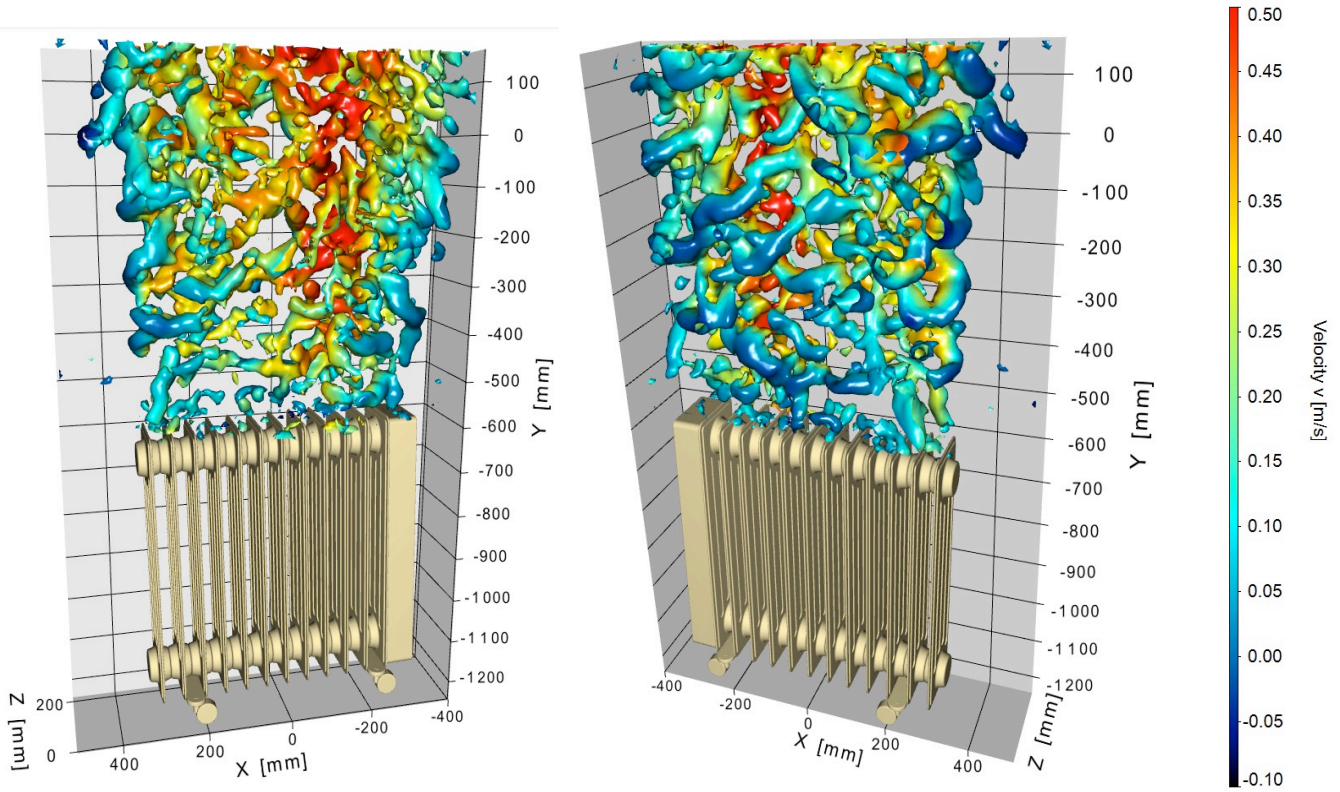
Figure. 7 Iso vorticity (λ_2, iso value = -2.0 1/s²) surfaces from binning (coloured by the vertical velocity component v). Left: view from the wall, right: view from the front.

Particle tracks from Shake-the-Box are converted to velocity vectors on a regular grid using two methods that have different advantages and disadvantages: binning and data assimilation (VIC#) [8]. Binning is a simple and fast method, where velocity on a regular grid is calculated in the following way:

1. Calculate the velocity at the location of each particle for a given time step by fitting a 2nd-order polynomial over 7 time-steps.
2. Divide the measurement volume into bins of 96³ voxel size with 75 % overlap of the boxes (resulting in a 24 voxel vector grid).
3. For each grid point/bin, fit a first order polynomial to the velocities from all particles in this box and evaluate the velocity from the resulting polynomial at the centre of each bin.

This procedure results in instantaneous velocity fields of 110 x 93 x 25 vectors for each time step with a vector spacing of 8.2 mm (Figure 7).

Often binning is applied by simply averaging the velocity distribution of all particles for a given bin. However, it was found that this leads to inconsistent velocities at the borders of the

illuminated volume, especially at the wall. There, the bins reach inside the wall, so that particles tend to lay on one side of a bin. Due to the strong gradient at the wall, the velocity at these grid points is overestimated by simple averaging. On the other hand, the 1st-order polynomial fit inside the bin, applied here, can model the gradient, resulting in a more precise estimation of the velocity at the central grid point position.

The significant advantage of binning is its fast processing (0.4 seconds per time step), whereas the main disadvantage is its poor spatial resolution, here 8.2 mm vector spacing.
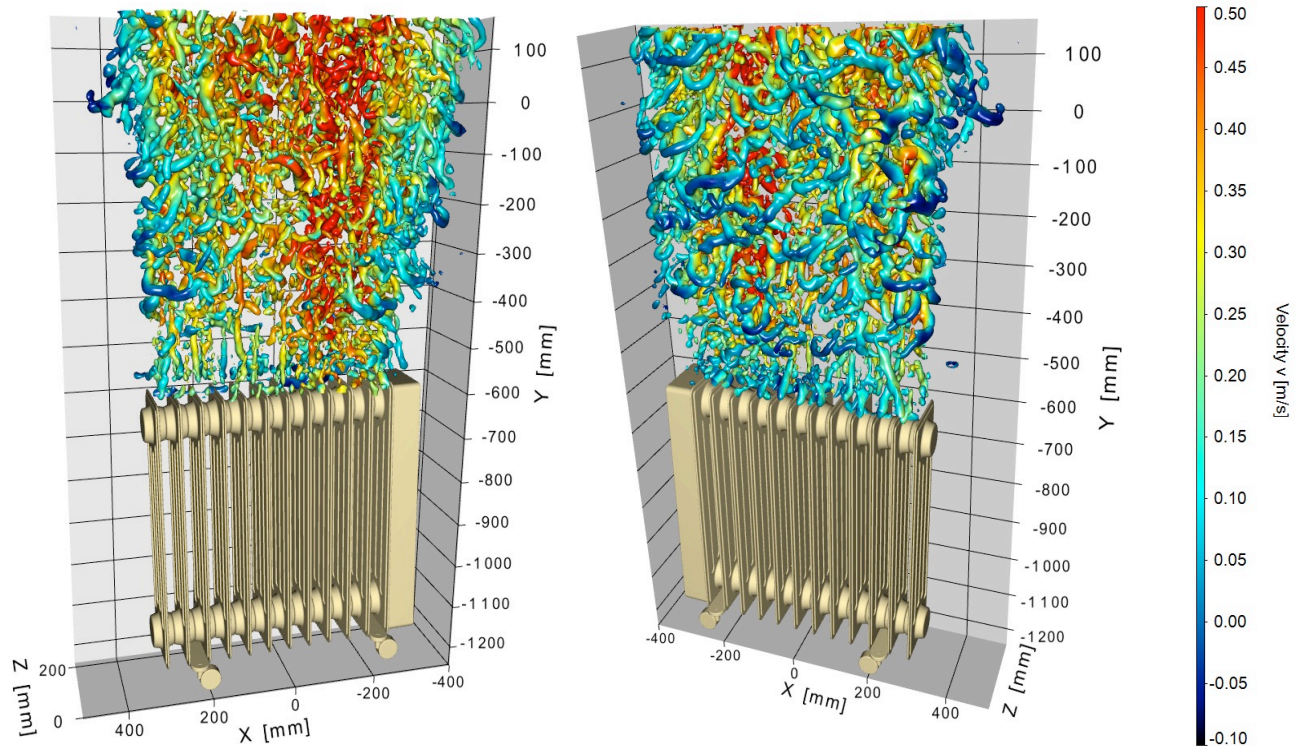
Figure. 8 Iso vorticity (λ_2, iso value = -20.0 1/s²) surfaces from data assimilation VIC# (coloured by the vertical velocity component v). Left: view from the wall, right: view from the front.

The data assimilation technique VIC# (Jeon 2022) uses physical constraints from the Navier-Stokes equation to find velocity vectors on a grid that fit both the physical constraints and the measured particle tracks. The result shows a considerably higher spatial resolution with a 4 mm vector grid resolving much finer details in the vortical flow structures (Figure 8). While the primary benefit of using VIC# is its high spatial resolution, the main drawback is the extensive computation time, requiring 23 minutes per time step.

4.3. Average velocity fields

Particle tracking allows the calculation of average velocity fields with high spatial resolution. With a given minimal number of particles that need to contribute to a bin for averaging (e.g. 50 particles

per bin), the bin size can be progressively reduced as the number of analysed time steps increases, thereby increasing the total number of tracked particles. Consequently, the bin size for averaging over 10000 time steps can be significantly smaller compared to averaging over only 500 time steps. Figure 9 shows the average velocity magnitude from 10000 time-steps, with a bin size of 24 x 24 x 24 voxel and 75% bin overlap resulting in 2 mm vector spacing and 439 x 370 x 100 velocity vectors. The smooth average corresponds to the physical expectation and exhibits detailed features at individual radiator ribs, the control box and a strong velocity gradient at the wall.
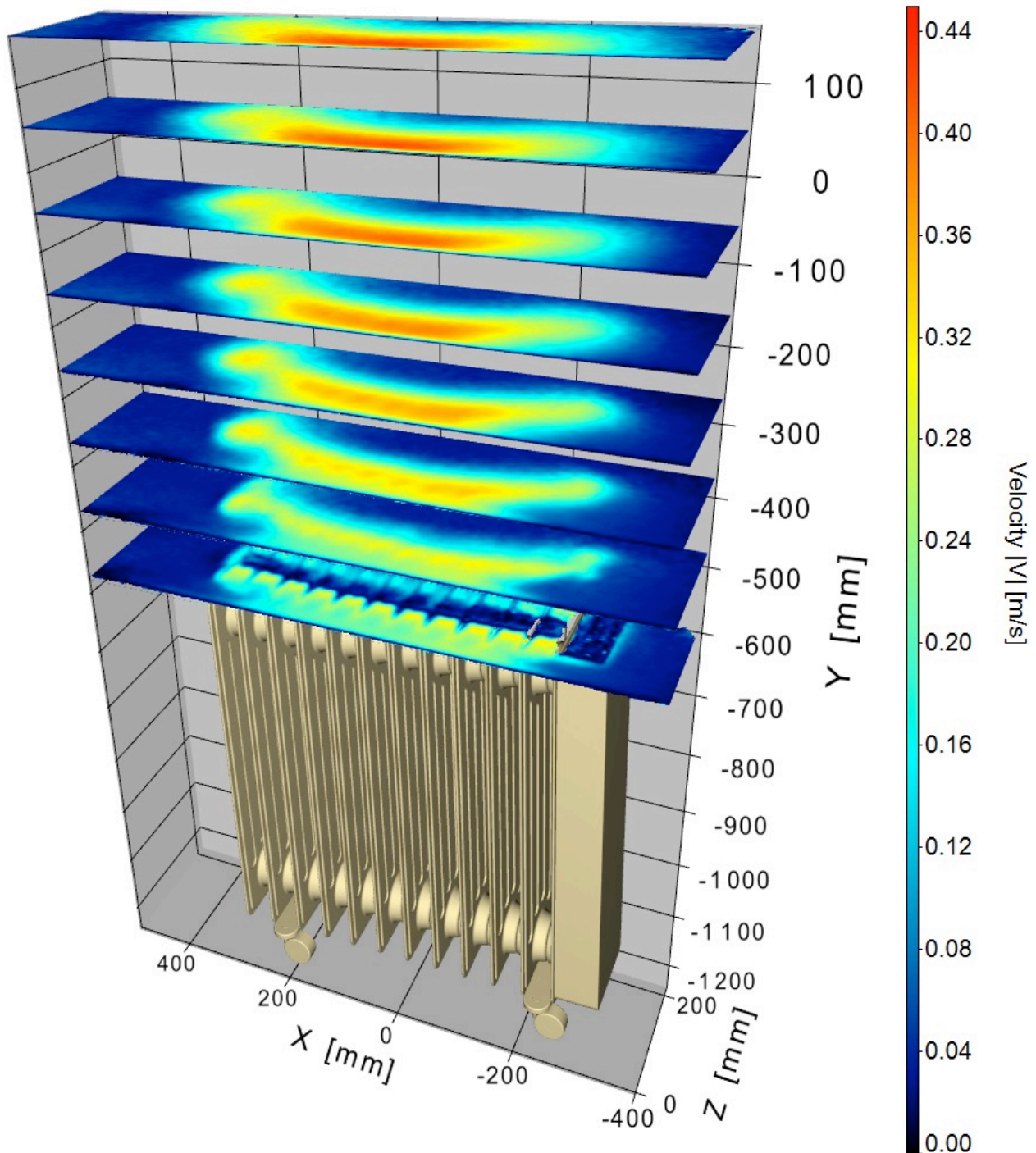
Figure. 9 Average velocity magnitude from average binning of 10000 time-steps.

Further details of the average vertical velocity component are displayed in Figure 10: As expected, the region of the highest upward velocity originates from the gap between the radiator and the wall (red regions in Figure 10). In the higher plane above the radiator, the flow is attached to the wall with a thin boundary only in the central part behind the radiator. Further to the sides the flow detaches and the region of highest vertical velocity moves away from the wall. In the lower plane, again, the imprint of the individual radiator fins and the control box on the flow is clearly visible. At the sides of the radiator the flow is slightly asymmetrical with a slow upward flow (light green) on the lefthand side and slow downward flow (light blue) at the righthand side.
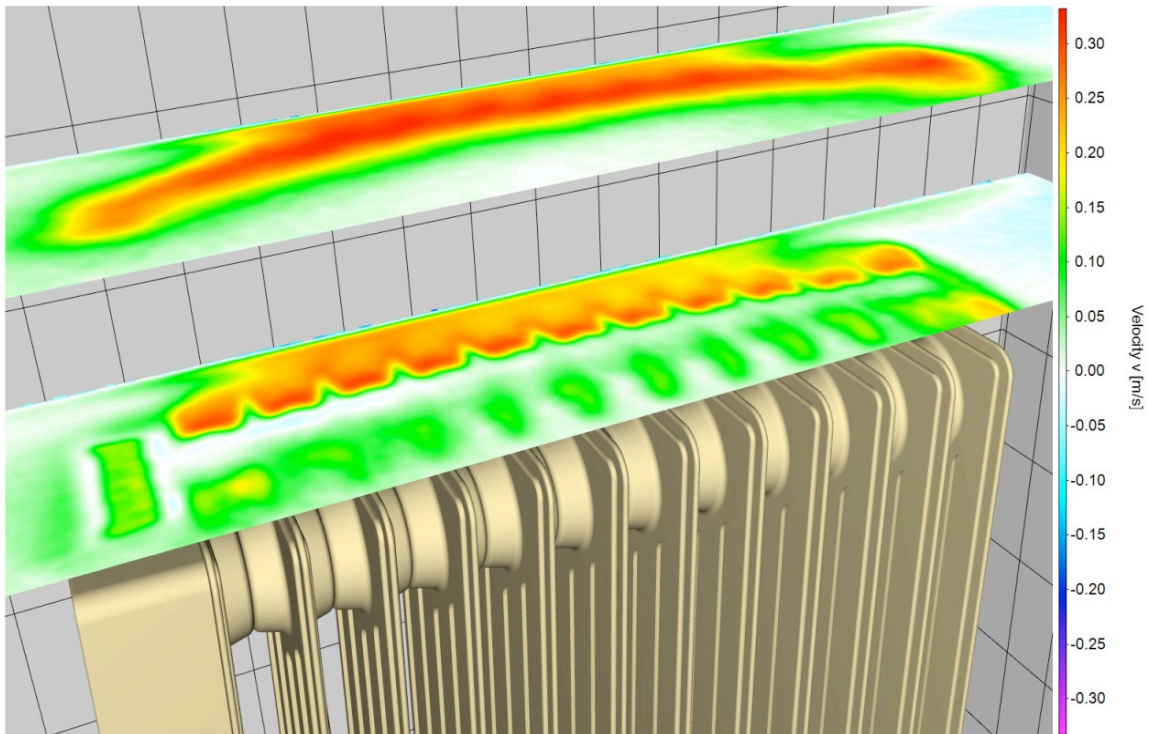
Figure. 10 Detail of the average vertical velocity component on top of the radiator. Note the imprint of the individual fins and the control box (on the lefthand side) as well as the thin shear layer at the wall.

The structure of the boundary and shear layers becomes more visible in the plot of the standard deviation of velocity (Figure 11). Very close to the radiator, the shear layer is very thin and modulated by the radiator fins. Further upstream, this shear layer is folding inwards at the sides forming two hook like structures. The highest standard deviation is observed in the boundary layer at the wall, showing an increasing thickness with the height, signifying a growing turbulent boundary layer. The wall region with the highest turbulence intensity (Figure 12) is also expected to be the zone of highest heat exchange with the wall.
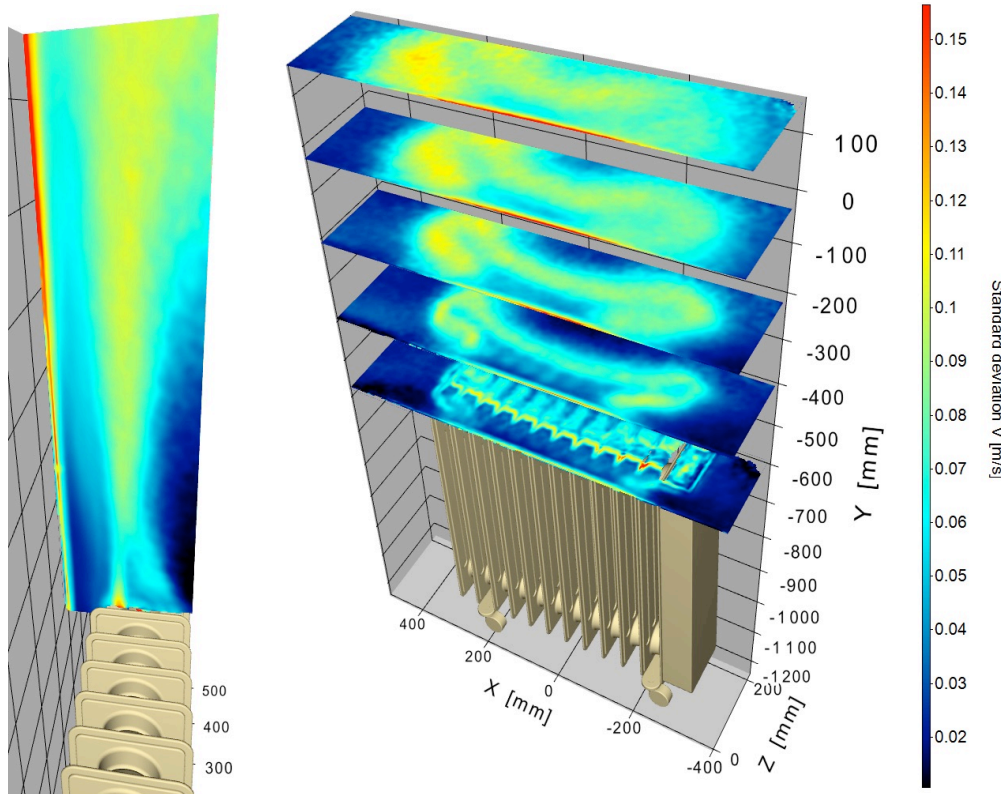
Figure. 11 Standard deviation of the velocity
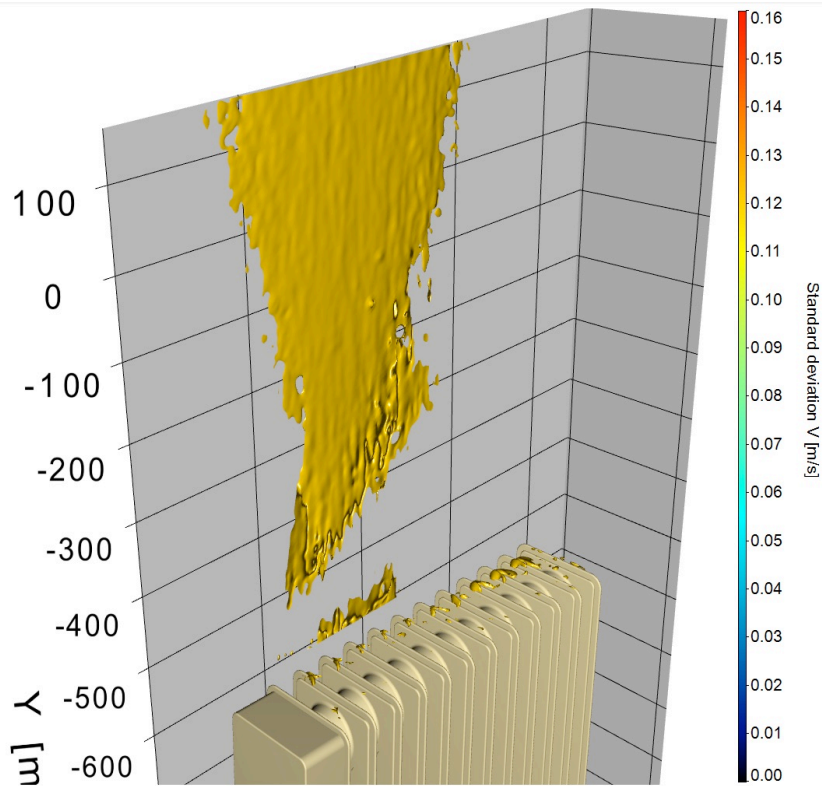
Figure. 12 Iso surface of the standard deviation of the velocity (iso value = 0.12 m/s): the turbulent boundary layer at the wall is expected to be the zone of highest heat exchange with the wall.

2D streamlines, calculated from a central plane of the average flow field, are very similar to the ones presented in the literature [1], serving as a sanity check of the present results (Figure 13).
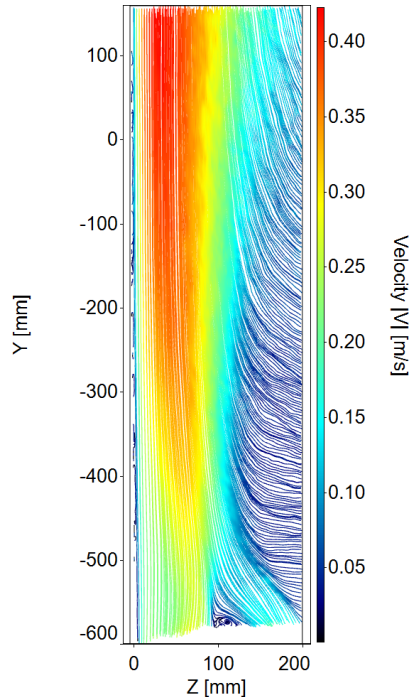
Figure. 13 2D streamlines from the central y-z plane.

50 particles per bin have been used as a minimum for accepting an average vector. To study the actual distribution of the number of particles per bin, this number is displayed in Figure 14. It is visible that up to 9000 particles contribute to a single vector, which is more than enough for statistical convergence. This indicates that there is potential for even smaller bins and a higher spatial resolution.
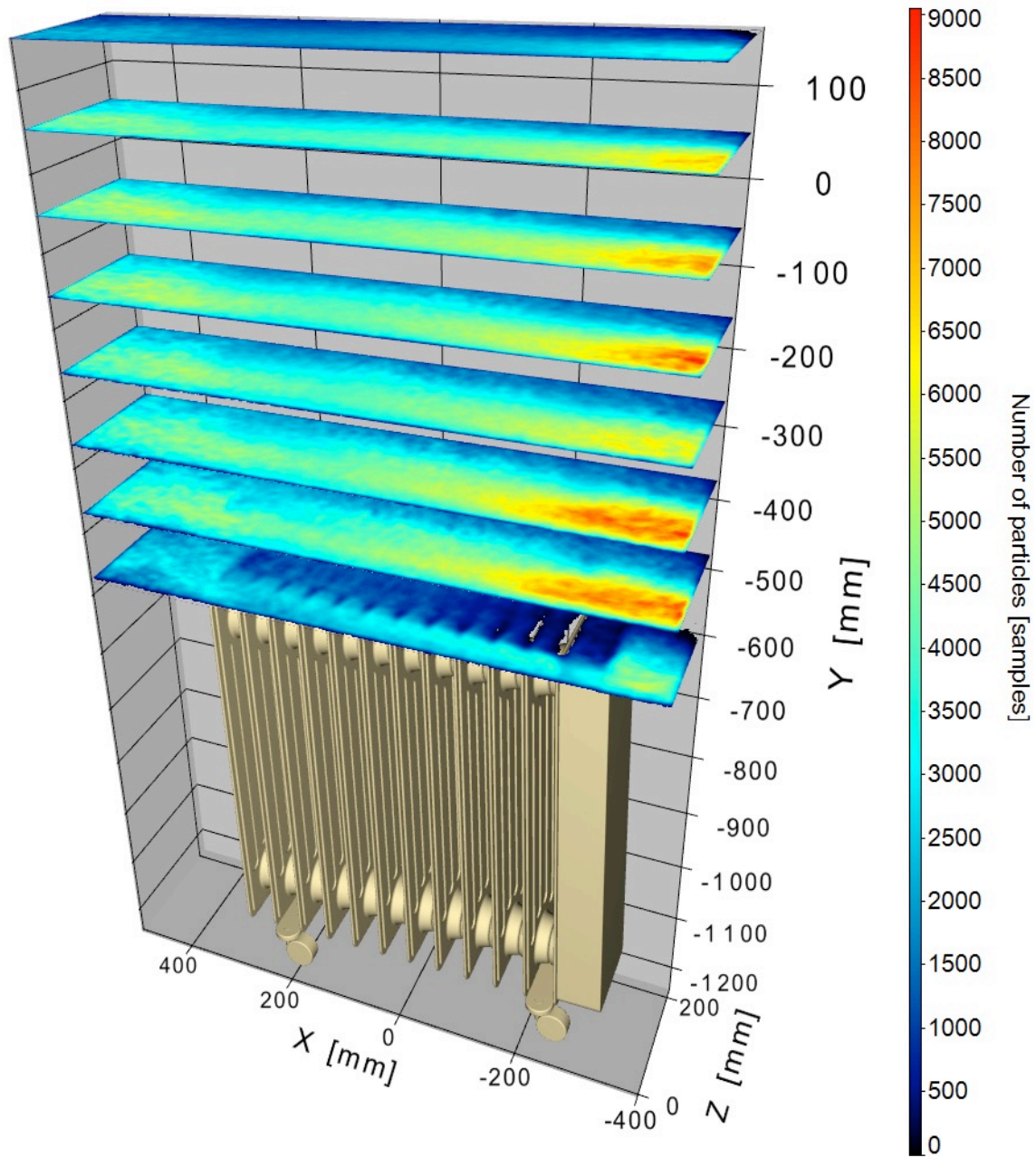
Figure. 14 Number of tracked particles that contribute to each average velocity vector with 2 mm vector spacing

Reducing the bin size from 24 x 24 x 24 voxel to 12 x 12 x 12 voxel (4 x 4 x 4 mm³) with 75% overlap results in a vector grid spacing of 1 mm (Figure 15, left) with still up to 650 particles per bin (Figure 15, right). With eight times fewer particles per bin, the velocity field now becomes more noisy, visible e.g. in the upper left corner where the number of particles per bin is relatively small. This signifies that the spatial resolution for the current measurements cannot be increased much further without accepting even higher noise levels.
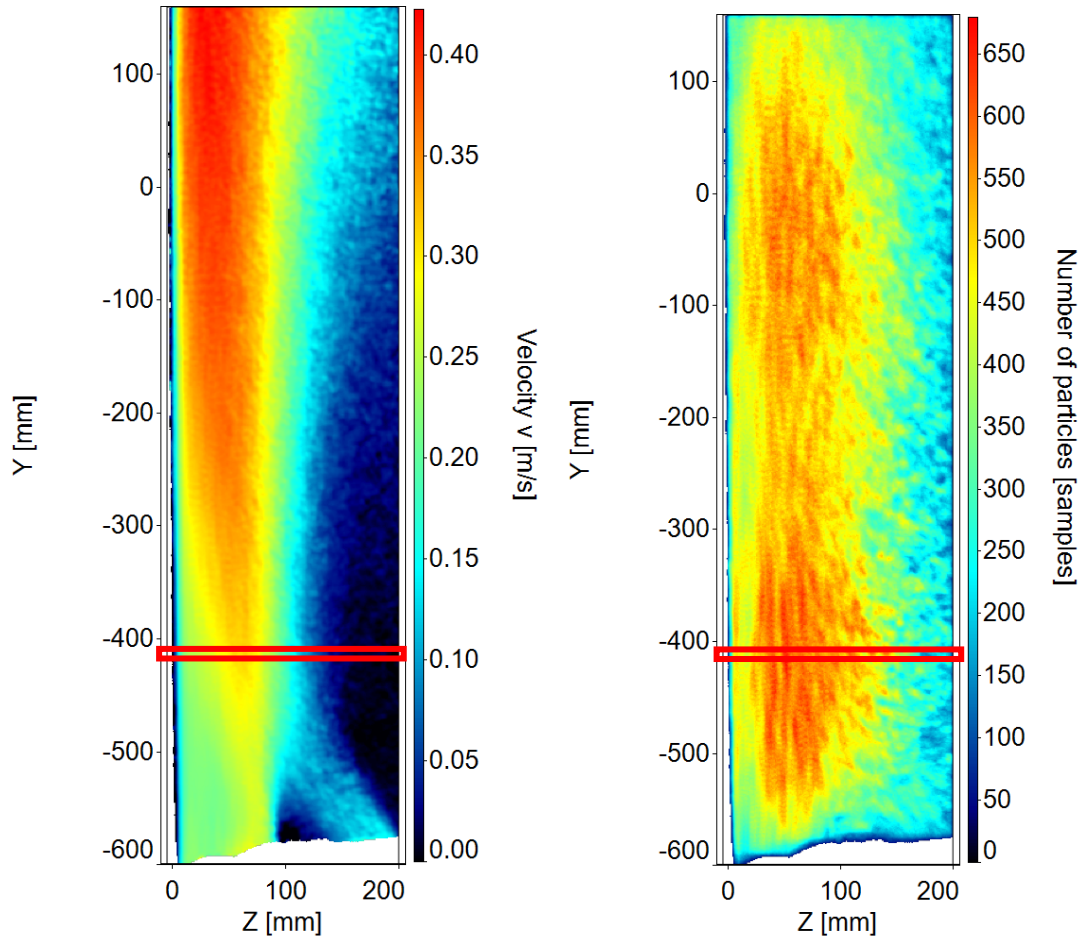
Figure. 15 average vertical velocity component (left) and corresponding number of particles per bin for 1 mm vector spacing.
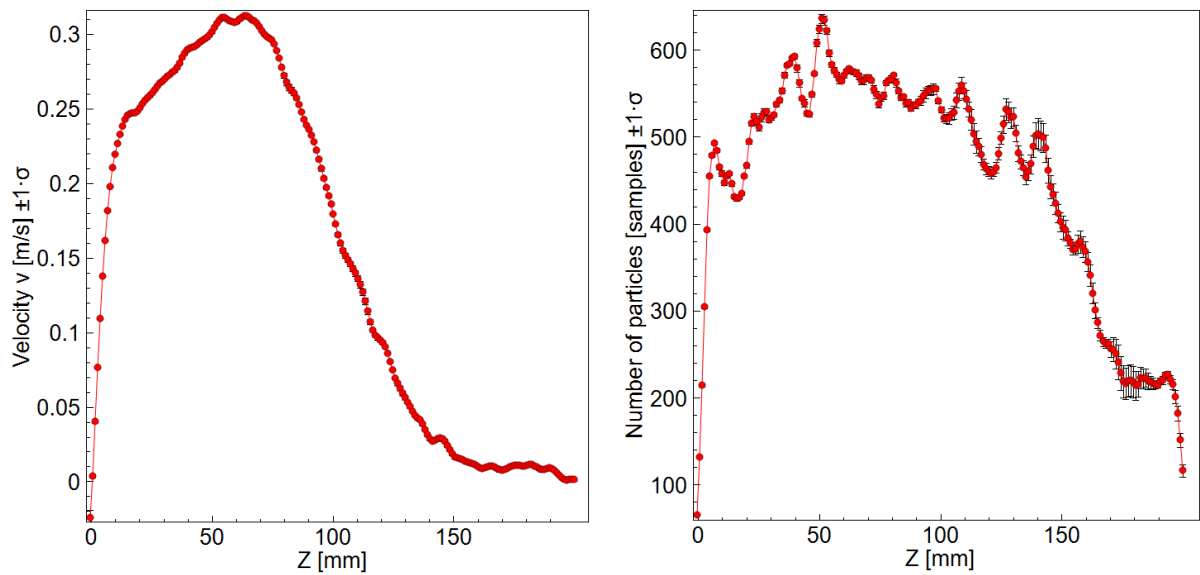
Figure. 16 Profiles of vertical velocity component (left) and number of particles per bin (right) along the z-direction (at the y position marked with the red rectangles in Figure 15).

Profiles of velocity and number of particles per bin are shown in Figure 16 to further investigate the flow behaviour close to the wall. This region is of special interest due to its major impact on the heat exchange between the wall and the flow. The velocity profile clearly shows that the thin boundary layer close to the wall is well resolved in the average flow field. The vertical velocity component even becomes negative at the smallest z coordinates. However, this could be an artefact from the first-order polynomial fit: As the wall position is not known with very high precision (the wall was also slightly curved), the grid point could reside within the wall, leading to negative vertical velocity components by extrapolation. Although some numerical flow simulations predict negative velocity components from a high density fluid cooled by the wall, further examination of individual particle tracks will be necessary to differentiate between an interpolation artefact and true downflow.

Close to the wall, the number of particles per bin is clearly decreasing to about 70 particles per bin, from more than 600 particles per bin away from the wall. This is somewhat expected, as it can be hard to get enough seeding particles inside the region very close to the wall due to the low velocity in this region. However, 70 particles per bin is considered enough to get a reliable velocity vector there. If necessary, this number could be increased in the future by recording more time steps.

Vortical structures

Vortical structures of the average flow field can be visualized using the λ_2 criterion (Figure 17). There, the iso surfaces of λ_2 are colour coded by the y component of vorticity. Vertically aligned vortices between the radiator fins at the wall side are formed, which rotate clockwise (red) or counter clockwise (blue). At the opposite side (away from the wall) these vortices are inclined by about 45° towards the radiator. Other dominant structures include four vortices originating from the four corners on the top of the radiator and a horizontal vortex at the side edge of the control box. To the authors knowledge these 3D details have not been measured before on a full scale radiator.
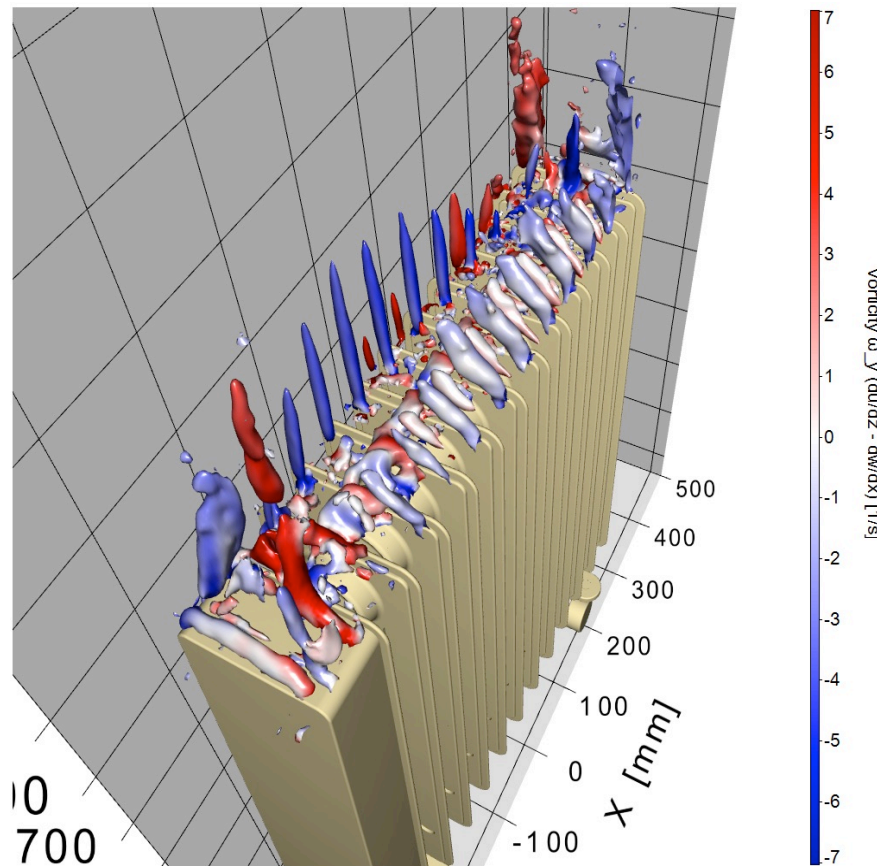
Figure. 17 Vortical structures from the average flow field on top of the radiator (iso surfaces of $\lambda_2 = -2.5\ 1/s^2$) colour coded by the y component of vorticity

4.4. Different background colours

In this section, the effect of the wall colour on particle tracking is investigated. The default colour of the walls in the future test chamber is white. The wall colour has an influence on heat transfer to and from the wall and especially on the light absorption if sunlight is to be simulated. For particle tracking, on the other hand, a black wall is preferred to avoid reflections of the LED light from the wall.

Recordings have been performed with a black wall (Figure 18, left) and a partly white wall (Figure 18, right). It is clearly visible that the background intensity is strongly increased by the white wall to about 30000 counts. The high dynamic range (16 Bit) of the sCMOS cameras still allows the detection of the much weaker particle signal on top of this background.
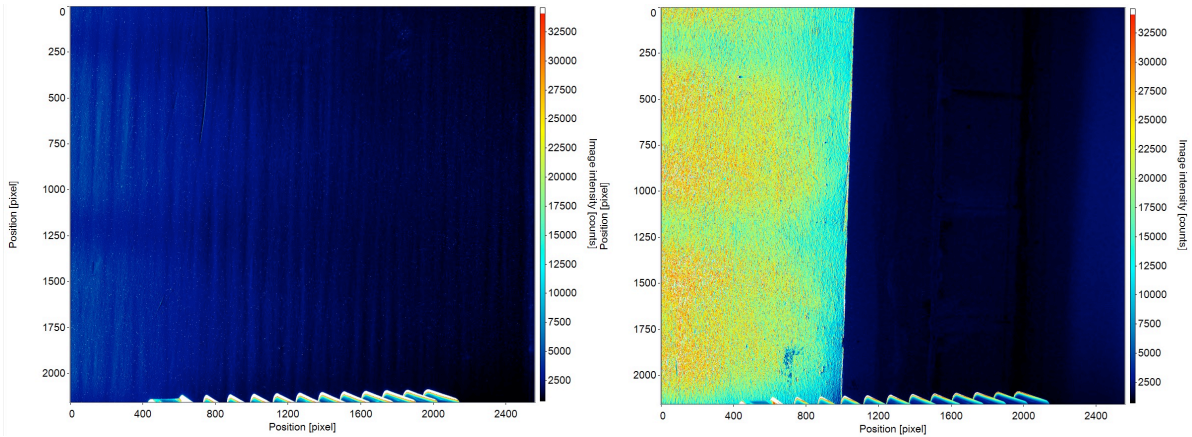
Figure. 18 raw images with black background (left) and partly white background (right).

To show the effect of the background colour, the tracked particles with their detected intensities are projected to the horizontal x-z plane. This allows to detect the distribution and intensity of the detected particles in this projected plane. For the black background (Figure 19a), it is found that the illuminated volume is smaller (smaller z range) close to the LEDs (at negative x) than further away from the light source (larger z range at positive x), which is caused by the divergent light source (opening angle about 5°). A similar effect is visible for the partly white background (Figure 19b), but another effect is more prominent in this case: The region in the red rectangle shows a high concentration of particles in a place where no particles are expected. These particles are ghost particles that result from the higher shot noise of the strong white background (remember that the wall is only white in the left half of the particle images). The same processing parameters have been used for cases a and b. To avoid the creation of ghost particles in front of the white background, a higher weighting factor for the subtraction of the sliding minimum is used (Figure 19c): 1.04 instead of 1.02, so that the higher shot noise is cancelled. This leads to the detection of fewer particles in the regions where the light intensity is low (away from the wall at positive z). However, the ghost particles have been eliminated successfully.

The resulting average velocity distribution (Figure 20) is very similar to the results with the black wall as background (Figure 9). The thin boundary layer at the wall and the small details on top of the radiator are still well resolved. The reduced depth of the measurement volume could be compensated in future experiments by increasing the distance of the LED's from the measurement volume, increasing the size of the light spot. This would also decrease the intensity of the particles and reflections, which should be acceptable here, given the relative high intensity level of the particles in the current measurements.
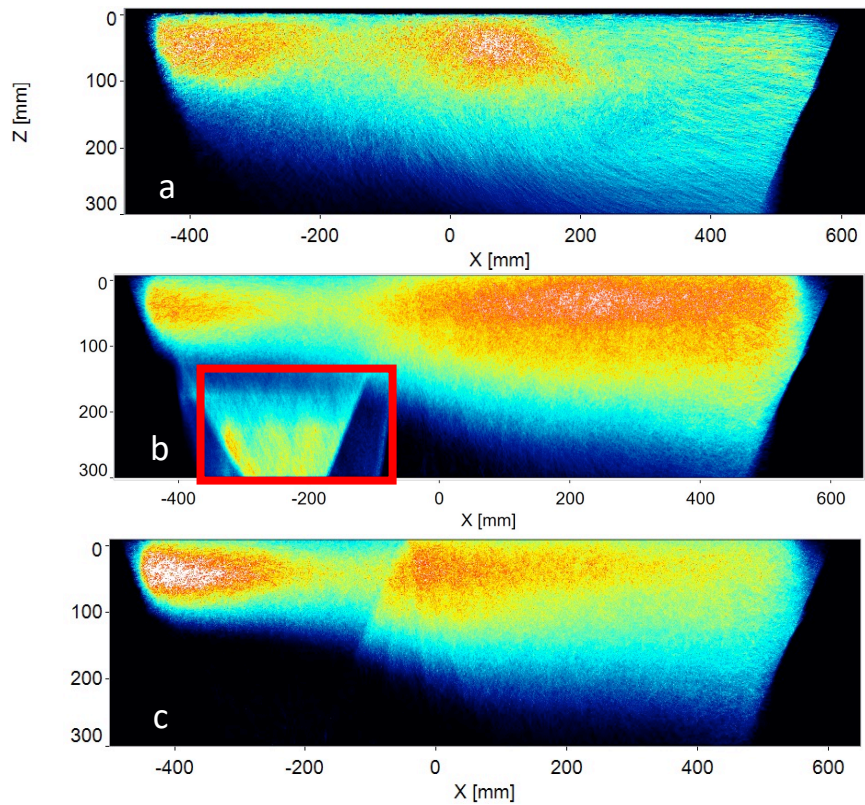
Figure. 19 vertical projections of detected particles and their intensity. a) black background, weak background subtraction, subtract-minimum-factor 1.02, b) and c) partly white background, b) weak background subtraction, subtract-minimum-factor 1.02, c) strong background subtraction, subtract-minimum-factor 1.04
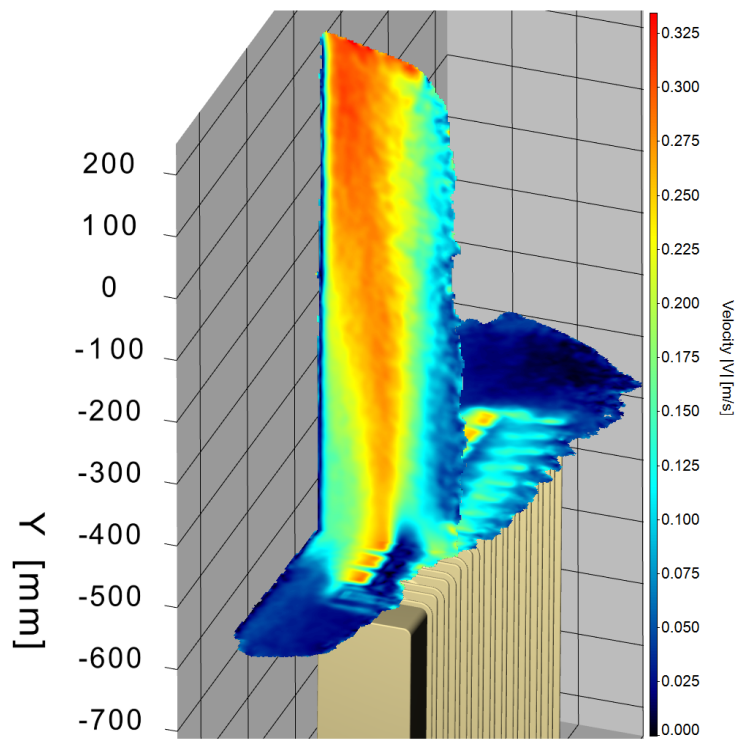
Figure. 20 Average velocity (3000 time steps) in a vertical and a horizontal plane (from recordings with white background)

5. Discussion

Results using a black wall colour are found to yield more particle tracks in a larger volume, because weak particles in the darker regions of the illuminated volume can be tracked more reliably using a less aggressive background subtraction. However, a black wall may alter the thermal properties considerably, especially when the absorption of sunlight is modelled in future experiments: All the energy in the (simulated) spectrum of the sun (Figure 21) will be absorbed by a black wall, leading to a considerable temperature change at the wall that could significantly alter the flow at the wall.

A practicable alternative to a black wall for this application could be the use of an orange wall colour, that selectively absorbs the blue light from the LED's, leaving the majority of the spectrum unaffected.
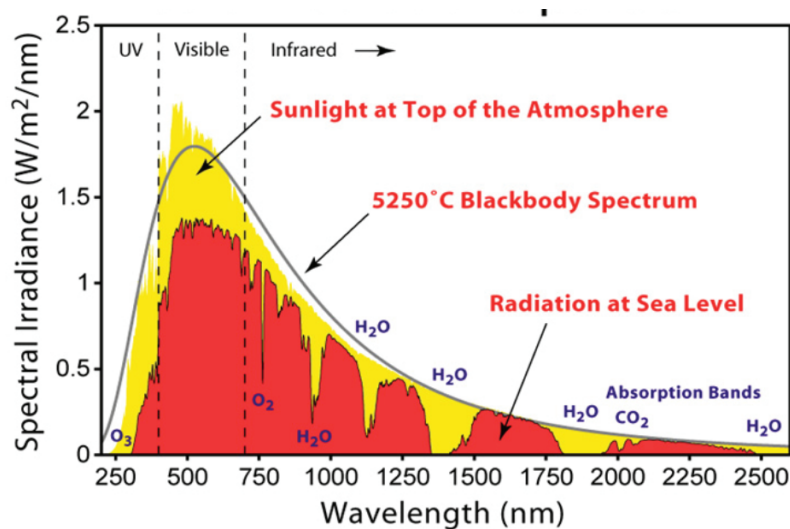
Figure. 21 Sun spectra above the atmosphere and at sea level, along with corresponding black body radiation (Ranabhat et al. 2016)

6. Conclusion

To the author's knowledge, the complete instantaneous volumetric flow on top of a radiator has been measured with high spatial resolution for the first time. The designed system for thermal convective flow measurements is found to yield very good results for velocity measurements with the desired spatial resolution of 1 mm for average flow fields and 4 mm for instantaneous velocity fields using data assimilation VIC#. Water cooling was found to be a valid approach to avoid the introduction of undesired flow from fans and additional heat sources in a confined chamber. A black background leads to more tracked particles in a larger volume. Results from a white

background are still very acceptable with a slightly smaller measurement volume. A wall colour absorbing only the blue LED's light is recommended for future measurements.

Acknowledgments

References

Jeon, Y.J., Müller, M. & Michaelis, D. (2022) Fine scale reconstruction (VIC#) by implementing additional constraints and coarse-grid approximation into VIC+. Exp Fluids 63, 70

Peng, Z., Carrigan, S., & Kornadt, O. (2023). Numerical investigation of the heat transfer in realistic rooms with a two-panel radiator. In: Building Simulation Conference Proceedings, Proceedings of the 18th International IBPSA Building Simulation Conference and Exhibition (pp. 1552–1559).

Peng, Z., Carrigan, S., & Kornadt, O. (2022). Local room-side heat transfer of an office room with different heating strategies. Bauphysik, 44(6), 317–322.

Posner, J.D., Buchanan, C.R., Dunn-Rankin, D. (2003) Measurement and prediction of indoor air flow in a model room, Energy and Buildings, Volume 35, Issue 5

Ranabhat, K., Patrikeev, L., Antal'evna-Revina, A., Andrianov, K., Lapshinsky, V., & Sofronova, E. (2016). An introduction to solar cell technology. Istrazivanja i projektovanja za privredu, 14(4), 481–491.

Sattari, A. (2015) Particle Image Velocimetry Visualization and Measurement of Airflow Over a Wall-Mounted Radiator, International Journal of Ventilation, 14:3, 289-302

Scarano, F., Ghaemi, S., Caridi, G.C.A. et al. (2015) On the use of helium-filled soap bubbles for large-scale tomographic PIV in wind tunnel experiments. Exp Fluids 56, 42.

Schanz, D., Gesemann, S. & Schröder, A. (2016) Shake-The-Box: Lagrangian particle tracking at high particle image densities. Exp Fluids 57, 70

Schröder, A., Schanz, D., Michaelis, D., Cierpka, C., Scharnowski, S., & Kähler, C. J. (2015) Advances of PIV and 4D-PTV" Shake-The-Box" for turbulent flow analysis–the flow over periodic hills. Flow, Turbulence and Combustion, 95, 193-209.

Schröder, A., Schanz, D., Bosbach, J., Novara, M., Geisler, R., Agocs, J., & Kohl, A. (2022) Large-scale volumetric flow studies on transport of aerosol particles using a breathing human model with and without face protections. Physics of Fluids, 34(3).

Wieneke, B. (2008) Volume self-calibration for 3D particle image velocimetry. Exp Fluids 45, 549–556